ROYAL SOCIETY OF CHEMISTRY

CrossMark
←click for updates

Stokes and anti-Stokes luminescence in Tm³⁺/Yb³⁺-doped Lu₃Ga₅O₁₂ nano-garnets: a study of multipolar interactions and energy transfer dynamics

Mamilla Rathaiah,[a] Pamuluri Haritha,[a] Antonio Diego Lozano-Gorrín,[b] Palamandala Babu,[c] Chalicheemalapalli Kulala Jayasankar,[d] Ulises Ruyman Rodríguez-Mendoza,[b] Victor Lavín[b] and Vemula Venkatramu*[a]

Nanocrystalline Lu₃Ga₅O₁₂ garnets doped with Tm³⁺/Yb³⁺ ions have been synthesized by a low cost and environmentally benign sol–gel technique and characterized for their structural, Stokes and anti-Stokes luminescence properties. The diffuse reflectance spectra of doped Lu₃Ga₅O₁₂ nano-garnets have been measured to derive the partial energy level structure of Tm³⁺ and Yb³⁺ ions and possible energy transfer channels between them. Upon laser excitation at 473 nm, weak red and intense near-infrared Stokes emissions have been observed in the nano-garnets. The decay curves of $^3H_4$ and $^1G_4$ levels of Tm³⁺ ions and the $^2F_{5/2}$ level of Yb³⁺ ions have been measured upon resonant laser excitation and are found to be non-exponential in nature due to multipolar interactions. In order to know the kind of multipolar interaction among optically active ions, the decay curves are analyzed through the generalized Yokota–Tanimoto model. Moreover, under 970 nm laser excitation, intense blue anti-Stokes emission is observed by the naked eye in Tm³⁺–Yb³⁺ co-doped Lu₃Ga₅O₁₂ nano-garnets. The results show that as-synthesized nano-garnets may be useful in the field of phosphors and photonics.

1. Introduction

Currently, research on lanthanide (Ln³⁺) doped oxide based nanocrystals is one of the burgeoning fields for the development of materials for optical sensors, phosphors in solid state lighting, display devices, photovoltaic and photocatalytic applications, *etc.*,[1–7] since the resolution is inversely related to the size of the particle.[8] All these applications could be realized through the control of the excited state dynamics of Ln³⁺ ions by choosing appropriate host matrices with optimized active ion concentrations. Different host materials bear different concentrations of active ions, diverse phonon energies, and energy transfer efficiencies, *etc.*, which play a vital role in luminescence properties of Ln³⁺ ions. Thus, it is of great importance to choose a suitable host material with critical active ion concentration. An ideal host material should exhibit: (i) high solubility of active ions, (ii) low phonon energy to minimize non-radiative relaxations, (iii) high transparency from UV to NIR regions and (iv) high chemical and thermal stabilities to retain the original crystal structure. To date, Ln³⁺-doped inorganic materials such as oxides, oxysulfides, oxysalts, oxyfluorides and fluorides have been investigated for specific applications.[4,9–12] Among different kinds of oxide host matrices, garnets are important due to their fascinating physical, chemical, and optical properties.[13,14] Especially, lutetium (Lu) based garnets are advantageous because top of the valence band is mainly composed of 4f [Lu] orbitals.[15] Therefore, the luminescence of Ln³⁺ ions in Lu based crystals would increase according to the intensity-borrowing mechanism.[16]

Among different Ln³⁺ ions, Ho³⁺, Er³⁺ and Tm³⁺ are commonly chosen as activators for upconversion (UC) luminescence due to their rich energy levels for radiative transitions. Particularly, the Tm³⁺ ion has great importance due to its ladder type metastable levels ($^1D_2$, $^1G_4$ and $^3H_4$) to give a wide range of visible-NIR emissions.[7] The UC luminescence of Tm³⁺ ions can be sensitized by Yb³⁺ ions through efficient energy transfer, since the Yb³⁺ ion has a large absorption cross-section at around 980 nm.[7,17] The 480 nm ($^1G_4 \rightarrow {}^3H_6$) UC emission might be useful in high-density optical data storage and to improve photocatalytic activity.[6,7] The luminescence at around 800 nm through $^3H_4 \rightarrow {}^3H_6$ transition can be used in quartz optical amplifier applications.[7]

[a] *Department of Physics, Yogi Vemana University, Kadapa 516 003, India.*
E-mail: vvramuphd@gmail.com
[b] *Departamento de Física, MALTA Consolider Team, IMN and IUdEA, Universidad de La Laguna, 38200 San Cristóbal de La Laguna, Santa Cruz de Tenerife, Spain*
[c] *Department of Physics, Govt. Degree College, Satyavedu-517 588, India*
[d] *Department of Physics, Sri Venkateswara University, Tirupati 517 502, India*

The 1800 nm emission can be used to enhance the efficiency of cascaded three-junction solar cells.[18]

The critical distance between optically active ions in host matrices plays a vital role in energy transfer (ET) and in deriving efficient luminescence from them for specific applications. Two types of ET processes may occur between Ln^{3+} ions: (a) resonant ET and (b) phonon assisted ET. Zheng *et al.* reported the role of phonon assisted energy transfer in converting visible light into infrared radiation in Tm^{3+}–Yb^{3+} co-doped YPO_4 powders.[19] Ganem *et al.* observed efficient emission at around 1800 nm in Tm^{3+} singly doped YCl_3 crystals due to the cross-relaxation ET process.[20] Mita *et al.* studied concentration dependent energy transfer processes in fluoride crystals co-doped with Tm^{3+}–Yb^{3+} ions, using the rate equation model and Monte Carlo simulation.[21] In this direction, it is quite interesting to investigate the ET processes between Tm^{3+} and/or Yb^{3+} ions in the LuGG nano-garnets using the Inokuti–Hirayama Model and the generalised Yokota–Tanimoto model (Martin model) to analyse the multipolar interactions.

The luminescence properties of Tm^{3+}/Yb^{3+}-doped phosphors such as $Lu_5O_4F_7$, LuF_3, YPO_4, $Y_3Al_5O_{12}$ (YAG), $Gd_3Ga_5O_{12}$ (GGG), $YAlO_3$, Y_2O_3, and Lu_2O_3 crystals have been studied.[11,12,19,22–26] Pandozzi *et al.*[23] studied Stokes and UC emission in Tm^{3+}–Yb^{3+} co-doped GGG nano-garnets and found that the addition of Yb^{3+} ions does not affect visible emission but NIR emission was affected due to back energy transfer (BET) between dopant ions ($Tm^{3+} \leftrightarrow Yb^{3+}$) under 465.8 nm laser excitation. Furthermore, the UC emission was found to contain intense blue and NIR emissions and weak red emission. Etchart *et al.*[27] synthesized the Tm^{3+}–Yb^{3+} co-doped Y_2BaZnO_5 phosphors *via* a solid state reaction method and studied their concentration dependent UC emission properties. So far there has been no report on the influence of concentration of Tm^{3+} ions on their luminescence and the effect of Yb^{3+} concentration on the UC luminescence of Tm^{3+} ions in $Lu_3Ga_5O_{12}$ (LuGG) nano-garnets. Moreover, the multipolar interactions among the optically active ions in the nano-garnets have not been studied in detail so far.

Hence, in the present work, Tm^{3+}-doped and Tm^{3+}–Yb^{3+} co-doped $Lu_3Ga_5O_{12}$ nano-garnet powders are successfully synthesized *via* a low cost, environmentally benign sol–gel method and their structural, optical and luminescence properties are studied through powder X-ray diffraction (XRD), dynamic light scattering (DLS), diffusion reflection spectroscopy, Stokes luminescence, decay and power-dependent anti-Stokes luminescence techniques. The non-exponential decay curves are analyzed in the frame of Inokuti–Hirayama and generalized Yokota–Tanimoto models to determine the kind of multipolar interaction, energy transfer and diffusion parameters.

2. Experimental section

Nano-garnets of composition $(Lu_{(1-x)}Tm_x)_3Ga_5O_{12}$ (where x = 0.01, 0.02, 0.03, 0.04 and 0.05, and hereafter denoted as LuGG1Tm, LuGG2Tm, LuGG3Tm, LuGG4Tm and LuGG5Tm, respectively) and $(Lu_{(1-x-y)}Tm_xYb_y)_3Ga_5O_{12}$ (where x = 0.01,

y = 0.01 and 0.1, and hereafter denoted as LuGG1Tm1Yb and LuGG1Tm10Yb) were synthesized through a sol–gel method in air atmosphere.[3] The XRD patterns of the as-synthesized nano-garnets were measured using the $CuK_{\alpha 1}$ (1.5406 Å) rays (power: $35 V \times 15 mA$) with a step size of $0.02°$ (RIGAKU; Miniflex-600). The size distribution of nano-garnets was characterized using a Zetasizer Nano-S90 (Malvern Instruments, USA) by the DLS technique. The diffuse reflectance spectra (DRS) in the UV-Visible-NIR region were measured using a spectrophotometer (Agilent Technologies Cary 5000). The Stokes photoluminescence spectra of the nano-garnets were measured in the range of 600–1900 nm by exciting at 473 nm using a diode pumped solid state laser (DPSSL). The upconversion (anti-Stokes) spectra were recorded in the range of 400–750 nm by exciting at 970 nm using a Ti:sapphire laser (Spectra Physics 3900S) pumped by a 532 nm Millennia laser (Spectra Physics). These emissions were focused by a converging lens onto a fiber coupled 0.303 m single grating spectrograph (Andor Shamrock SR-303i-B) and then detected using a cooled CCD detector (Newton DU920N). The luminescence decay curves of $^3H_4$ and $^1G_4$ levels of Tm^{3+} ions were measured under 685 and 463 nm laser excitations, respectively, using a 10 ns optical parametric oscillator (EKSPLA/NT342/3/UVE) equipped with a single-grating monochromator (Jobin-Yvon TRIAX180) coupled to a PMT (Hamamatsu R928) and a digital storage oscilloscope (Tektronix 2430). The $^2F_{5/2}$ (Yb^{3+}) decay curves were measured under 930 nm laser excitation by monitoring the emission at 990 nm. All the measurements were carried out at room temperature and corrected for instrument response.

3. Results and discussion

3.1. Structural properties

The powder XRD patterns (see Fig. 1) of LuGG1Tm, LuGG5Tm and LuGG1Tm10Yb nano-garnets reveal that all of the reflections in the profiles of the powder samples are well-indexed to a single phase cubic structure, belonging to the $Ia\bar{3}d$ space group (No. 230) [ICDD database no. 01-073-1372]. The diffraction data are refined by the Rietveld fitting using the FULLPROF program.[28,29] Table 1 shows unit cell parameters and the corresponding goodness of fit (see reliability factors: χ^2, R_p, R_{wp}, and R_{exp}), and only minute differences are found in the amplitudes of few peaks (see Fig. 1). The high intensity diffraction peak centered at $32.5°$ is slightly shifted towards the lower angle side with dopant concentration, which may be due to the expansion of the lattice.[30] The LuGG garnet crystal structure is described as a three dimensional network with GaO_6 octahedra and GaO_4 tetrahedra linked by sharing oxygen ions at the corners of the polyhedral. These polyhedra have chain formation along three crystallographic directions to create dodecahedral cavities which are occupied by the Ln^{3+} ions.[3] The average crystallite size of samples is calculated by Scherrer's equation[13] and is found to be around 30 nm.

The lattice parameter is more or less similar upon substitution of ions.[14] A slight change in the unit cell parameter with dopant concentration can be ascribed to the changes in the position of
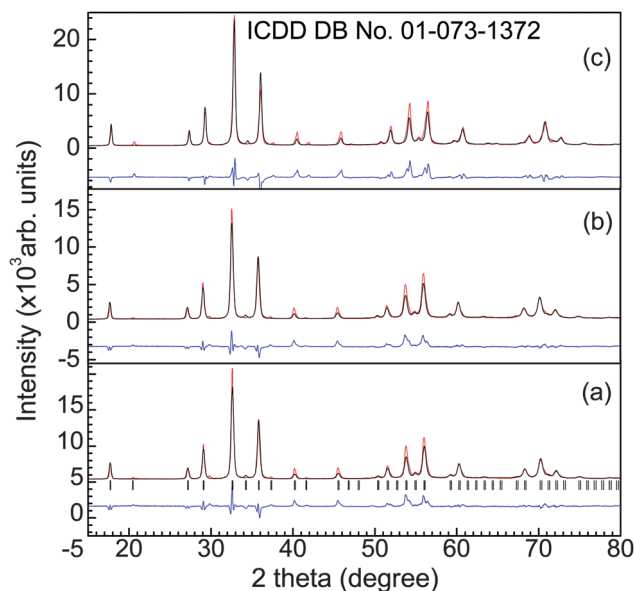
Fig. 1 X-ray diffraction patterns of (a) LuGG1Tm, (b) LuGG5Tm and (c) LuGG1Tm10Yb nano-garnets. Rietveld refinements including the differences (blue) between calculated (red) and observed (black) patterns are also shown. The vertical lines are the allowed reflections for this material in the $Ia\bar{3}d$ (No. 230) space group.

Table 1 Structural properties (lattice parameter and Rietveld refinement parameters) of Tm^{3+}/Yb^{3+}:LuGG nano-garnets

System	a (Å)	χ^2	R_p	R_{wp}	R_{exp}
LuGG1Tm	12.280	1.75	10.4	14.0	3.35
LuGG2Tm	12.284	1.99	11.0	14.6	3.26
LuGG3Tm	12.292	1.93	10.9	14.5	3.31
LuGG4Tm	12.294	2.20	11.5	15.0	3.20
LuGG5Tm	12.293	1.79	10.3	13.8	3.26
LuGG1Tm1Yb	12.241	3.78	13.7	18.0	2.92
LuGG1Tm10Yb	12.202	3.56	13.2	17.3	2.90

oxygen ions since the oxygen ion can be easily polarizable due to its relatively low electron density and size. The higher concentration of Ln^{3+} ions leads to higher deformation of the oxygen ions.[31] In Er^{3+}/Yb^{3+} doped YAG single crystals, it was reported that the lattice parameters were influenced by the motion of the oxygen ions.[31] A similar kind of effect may be expected with gallium ions in Tm^{3+}/Yb^{3+} doped LuGG nano-garnets.

The size distribution of the particles was analyzed using the DLS technique. The average diameter of the particle (d_p) is calculated using the Stokes–Einstein equation,[32]

$$d_p = \frac{kT}{3\pi\mu D} \tag{1}$$

where 'k' is Boltzmann's constant (J K^{-1}), 'T' is the absolute temperature (K), 'μ' is the viscosity of the medium (kg m^{-1} s^{-1}) and 'D' is the diffusion coefficient. The size distribution histogram of nano-garnets, shown in Fig. 2, reveals that they are grown in different sizes ranging from 15 to 90 nm. The maximum numbers of nano-garnets are grown to around
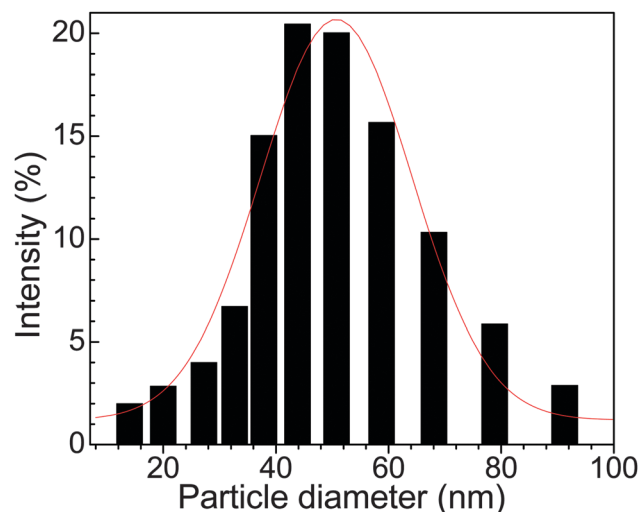

Fig. 2 Particle size distribution histogram of LuGG1Tm nano-garnets.

45 nm in size which is in good agreement with XRD results. Similar results are observed for all the titled nano-garnets.

3.2. Diffuse reflectance spectra

The DRS of LuGG5Tm and LuGG1Tm10Yb nano-garnets in the UV-visible-NIR regions are shown in Fig. 3. The observed peaks correspond to intra-configurational 4f–4f electronic transitions originating from the ground state to different excited levels of Tm^{3+}/Yb^{3+} ions. Fig. 3(a) corresponds to DRS of LuGG5Tm nano-garnets, which consists of seven absorption peaks centered at about 359, 464, 685, 810, 1208, 1420 and 1687 nm corresponding to the $^3H_6 \rightarrow {}^1D_2$, $^1G_4$, $^3F_{2,3}$, $^3H_4$, $^3H_5$ and $^3F_4$ transitions, respectively. In the case of LuGG1Tm10Yb nano-garnets (see Fig. 3b), in addition to the above mentioned transitions, a broad peak is observed in the region of 900–1050 nm due to the $^2F_{7/2} \rightarrow {}^2F_{5/2}$ transition of Yb^{3+} ions. The labels for transitions of Tm^{3+} and Yb^{3+} ions in the LuGG nano-garnets are assigned according to the notable Dieke's diagram
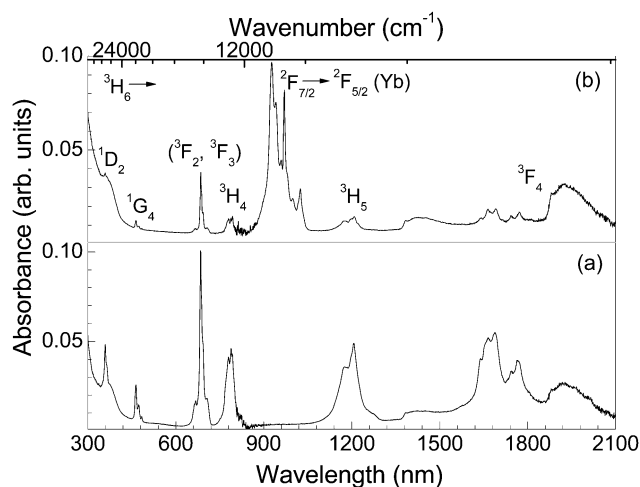

Fig. 3 Diffuse reflectance spectra of (a) LuGG5Tm and (b) LuGG1Tm10Yb nano-garnets.
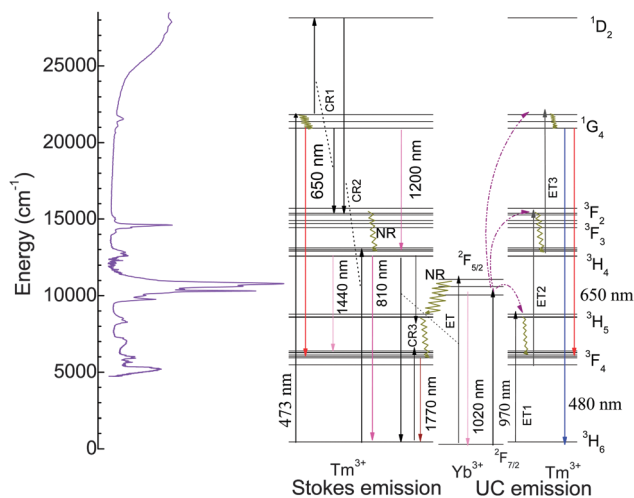
Fig. 4 Diffusion reflectance spectrum and the schematic partial energy level diagram showing radiative, non-radiative transitions, possible cross-relaxation and energy transfer channels for Stokes and UC emission in Tm^{3+}/Yb^{3+} doped LuGG nano-garnets.

for Tm^{3+} and Yb^{3+} ions in the $LaCl_3$ crystal.[33] The partial energy level diagrams of Tm^{3+} and Yb^{3+} ions have been derived from their DRS and are shown in Fig. 4, together with radiative and non-radiative transitions.

3.3. Luminescence

Visible and NIR Stokes luminescence spectra of LuGG1Tm, LuGG3Tm, and LuGG5Tm nano-garnets are measured exciting at 473 nm and are shown Fig. 5 for the region between 620–870 nm.
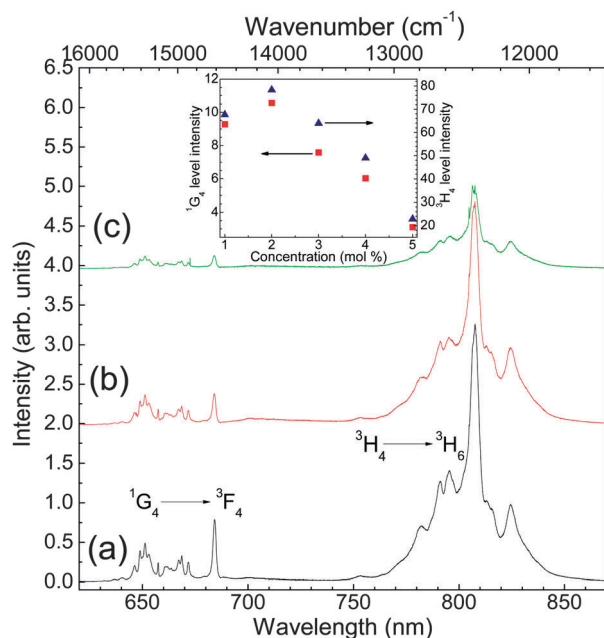

Fig. 5 Stokes emission spectra of (a) LuGG1Tm, (b) LuGG3Tm, and (c) LuGG5Tm nano-garnets (λ_{exc} = 473 nm). The inset shows variation in Stokes emission intensity from $^1G_4$ (■) and $^3H_4$ (▲) levels with respect to Tm^{3+} ion concentration.
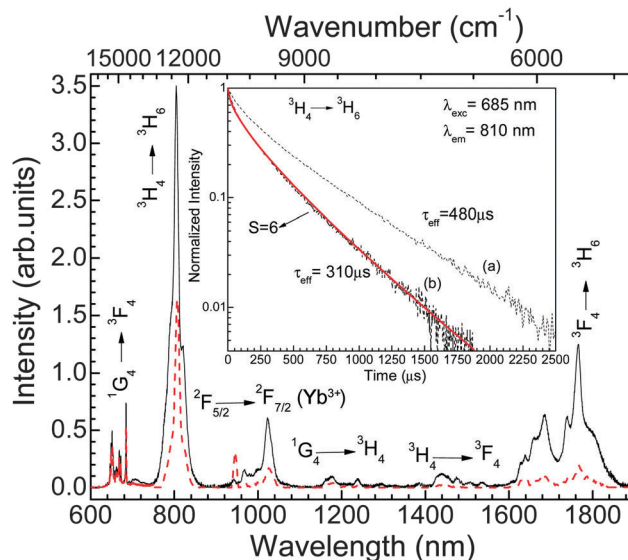

Fig. 6 Stokes emission spectra of LuGG1Tm1Yb (solid) and LuGG1Tm10Yb (dotted) nano-garnets (λ_{exc} = 473 nm). The inset shows Tm^{3+} luminescence decay curves of the $^3H_4$ level in (a) LuGG1Tm1Yb and (b) LuGG1Tm10Yb nano-garnets with IH model fitting (solid) for S = 6.

The red emission (640–680 nm) and a dominant NIR emission (760–840 nm) are assigned to $^1G_4 \rightarrow {}^3F_4$ and $^3H_4 \rightarrow {}^3H_6$ transitions, respectively. In the case of Tm^{3+}–Yb^{3+} co-doped nano-garnets, in addition to the above mentioned emissions, there are emissions at around 1020, 1200, 1440, and 1770 nm, which are ascribed to the $^2F_{5/2} \rightarrow {}^2F_{7/2}$ (Yb^{3+}), $^1G_4 \rightarrow {}^3H_4$, $^3H_4 \rightarrow {}^3F_4$, and $^3F_4 \rightarrow {}^3H_6$ transitions of Tm^{3+} ions, respectively (see Fig. 6). The sharp nature of all peaks is an indication of crystalline nature and occupation of the dopants at the Lu^{3+} sites.[3] The mechanism of various emissions can be explained as follows. When excited with a 473 nm laser, Tm^{3+} ions will be directly excited to the $^1G_4$ level. Then, some ions will be relaxed to the $^3F_4$ level by giving weak red emission. For the strong NIR emission at around 810 nm, there are two cross relaxation (CR) channels present to populate the $^3H_4$ level (see Fig. 4), CR1: $(^1G_4, {}^1G_4) \rightarrow ({}^3F_2, {}^1D_2)$, and CR2: $(^1D_2, {}^3H_6) \rightarrow ({}^3F_2, {}^3H_4)$.

The $^1D_2 \rightarrow {}^3F_2$ transition provides the energy to give $^3H_6 \rightarrow {}^3H_4$ transition, which populates the $^3H_4$ level via the $^3F_2$ level through non-radiative decay. Thus, one can observe strong NIR emission through $^3H_4 \rightarrow {}^3H_6$ transition. As shown in the inset of Fig. 5, above 2.0 mol% of Tm^{3+} ions, intensities of both red and NIR emissions diminish, which could be due to energy transfer through CR and diffusion among Tm^{3+} ions. In addition to CR1 and CR2 channels, there is one more phonon-assisted CR channel [CR3: $(^3H_4, {}^3H_6) \rightarrow ({}^3H_5, {}^3F_4)$ – 1300 cm^{-1} (absorbed from the lattice)] contributing to the emission process. The observed emission transitions have been described as follows (see Fig. 4):

Step 1: upon 473 nm laser excitation, Tm^{3+} ions are excited to the $^1G_4$ level, and then a few of them de-excite to the $^3F_4$ level to give weak red emission in the 640–690 nm range.

Step 2: CR1 and CR2 channels populate the $^3H_4$ level after non-radiative decay from $(^3F_2, {}^3F_3)$ levels. These two CR

This journal is © the Owner Societies 2016

Phys. Chem. Chem. Phys., 2016, 18, 14720–14729 | 14723

channels are responsible for dominant NIR emission in the range of 750–850 nm due to $^3H_4 \rightarrow {}^3H_6$ transition.

Step 3: due to phonon assisted energy transfer, some of the energy emitted from $^3H_4 \rightarrow {}^3H_6$ (Tm^{3+}) transition is transferred to nearby Yb^{3+} ions to excite them into the $^2F_{5/2}$ level and their de-excitation gives emission in the 950–1050 nm range through $^2F_{5/2} \rightarrow {}^2F_{7/2}$ transition.

Step 4: transition $^1G_4 \rightarrow {}^3H_4$ gives weak emission at 1200 nm.

Step 5: transition $^3H_4 \rightarrow {}^3F_4$ gives weak emission at 1440 nm.

Step 6: the BET channel $Yb^{3+}(^2F_{5/2}) \rightarrow Tm^{3+}(^3F_4)$, CR3 and non-radiative transitions from upper levels of the $^3F_4$ level will populate more heavily to give broad and intense emission in the 1600–1840 nm range from different Stark levels of the $^3F_4$ level to the $^3H_6$ level.

Pandozzi et al.[23] reported that under 465.5 nm laser excitation, the 1Tm^{3+}/1Yb^{3+} co-doped $Gd_3Ga_5O_{12}$ (GGG1Tm1Yb) nano-garnets exhibit strong blue-green (485 nm), considerable red (640–680 nm) and NIR (810 nm) emissions. They also observed strong emission from Yb^{3+} ions at around 1000 nm which is due to energy transfer from Tm^{3+} to Yb^{3+} ions. Li et al.[34] reported strong emission at around 650 and 1000 nm but weak peaks at around 800 and 1600 nm in Tm^{3+}/Yb^{3+} co-doped $CaSc_2O_4$ phosphors, under 466 nm laser excitation. But in LuGG1Tm1Yb nano-garnets, weak emission at around 1000 nm is observed due to energy transfer from $Tm^{3+} \rightarrow Yb^{3+}$ and emission between 1150 and 1800 nm are due to $^1G_4 \rightarrow {}^3H_4$, $^3H_4 \rightarrow {}^3F_4$, and $^3F_4 \rightarrow {}^3H_6$ transitions of Tm^{3+} ions. Whereas in LuGG1Tm10Yb nanogarnets, red emission is not affected upon increase in Yb^{3+} concentration because the 473 nm laser radiation cannot resonantly excite the Yb^{3+} ions.[35] Moreover, there are similar concentrations of Tm^{3+} ions in both the co-doped nano-garnets. But, NIR emission is strongly influenced by increasing the Yb^{3+} concentration as its intensity decreases very rapidly due to the transfer of energy between dopants through CR3 and $[Yb^{3+}(^2F_{5/2}), Tm^{3+}(^3H_6)] \rightarrow [Yb^{3+}(^2F_{7/2}), Tm^{3+}(^3H_5)] \pm h\nu$ (1600 cm^{-1}) channels (see Fig. 4) by dissipating/absorbing 2–3 host lattice phonons (LuGG $\sim$765 cm^{-1}) to/from the lattice.[3]

3.4. Decay curves

(i) $^3H_4$ (Tm^{3+}) level. The luminescence decay curves of the $^3H_4$ (Tm^{3+}) level in Tm^{3+} singly doped (see Fig. 7) and Tm^{3+}–Yb^{3+} co-doped (see the inset of Fig. 6) LuGG nano-garnets were measured at 685 nm laser excitation $[^3H_6 \rightarrow (^3F_2, {}^3F_3)]$ by monitoring the emission $[^3H_4 \rightarrow {}^3H_6]$ at 810 nm. All the decay curves exhibit non-exponential nature. Hence, the effective lifetime (τ_{eff}) of the $^3H_4$ level is evaluated by using the equation,[3]

$$\tau_{eff} = \frac{\int tI(t)dt}{\int I(t)dt} \qquad (2)$$

and all lifetime values of the $^3H_4$ level are shown in Table 2 for all the synthesized nano-garnets. It is found that for Tm^{3+} singly doped LuGG nano-garnets, the τ_{eff} decreases from 520 to 28 µs as Tm^{3+} ion concentration increases from 1.0 to 5.0 mol%. Armagan et al. reported a similar trend in Tm^{3+}-doped YAG crystals,
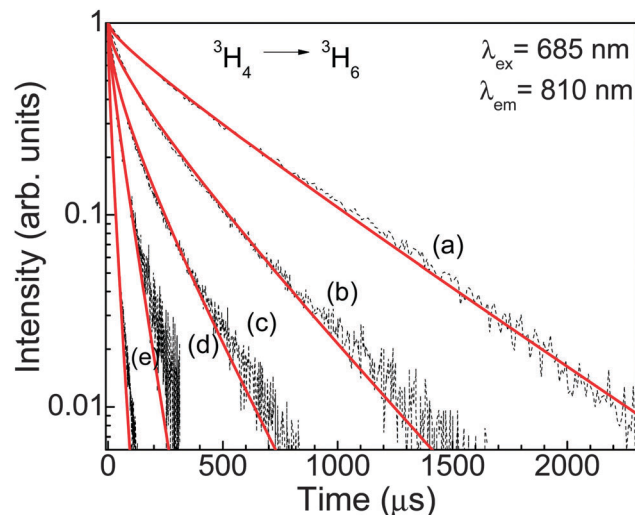

Fig. 7 Decay curves of the $^3H_4$ level of Tm^{3+} ions in (a) LuGG1Tm (b) LuGG2Tm, (c) LuGG3Tm, (d) LuGG4Tm and (e) LuGG5Tm nano-garnets under resonant excitation. The Martin model fitting (solid line) for $S = 6$ is shown for all nano-garnets.

Table 2 Lifetimes of the $^3H_4$ and $^1G_4$ levels of Tm^{3+}/Yb^{3+}:LuGG nano-garnets along with reported values in different hosts

System	Lifetime (µs)		Ref.
	$^3H_4$	$^1G_4$	
LuGG1Tm	520	320	Present
LuGG2Tm	280	153	Present
LuGG3Tm	150	74	Present
LuGG4Tm	60	42	Present
LuGG5Tm	28	22	Present
LuGG1Tm1Yb	480	290	Present
LuGG1Tm10Yb	310	270	Present
1Tm:YPO_4	—	100	19
1Tm/5Yb:YPO_4	—	85	19
1Tm:GGG nano-garnets	—	442	23
Tm/Yb:GGG nano-garnets	—	426	23
1Tm:$YAlO_3$	—	59	24
1Tm:Y_2O_3 nano crystals	—	135	25
1Tm/10Yb:Y_2BaZnO_5	—	125	27
1Tm:YAG	420	—	36
1Tm:YVO_4	100	—	37
1Tm:Y_2O_3 ceramics	192	92	38
1Tm/1Yb:Y_2O_3 ceramics	123	79	38
1Tm/5Yb:$YAl_3(BO_3)_4$	138	100	39
1Tm:$GdAl_3(BO_3)_4$	—	138	47
1Tm/1Yb:$GdAl_3(BO_3)_4$	—	130	47

where the τ_{eff} of the $^3H_4$ level decreased from 420 to 25 µs with increase in Tm^{3+} concentration.[36] In the case of Tm^{3+}–Yb^{3+} co-doped LuGG nano-garnets, the lifetime is found to decrease from 480 to 310 µs with increase in Yb^{3+} ion concentration from 1.0 to 10.0 mol%. A considerable decrease in the lifetime of the $^3H_4$ level is observed for the 1.0 mol% of Yb^{3+} ion co-doped nano-garnets compared to 1.0 mol% Tm^{3+}-singly doped nano-garnets indicating that there is energy transfer from Tm^{3+} ($^3H_4$) to Yb^{3+} ($^2F_{5/2}$). The τ_{eff} of the $^3H_4$ level in LuGG nano-garnets is found to be higher than those of Tm^{3+}-doped YAG, YVO_4 crystals, Y_2O_3 ceramics, and Tm^{3+}–Yb^{3+} co-doped Y_2O_3 ceramics and $YAl(BO_3)_4$ crystals (see Table 2).[36–39] The efficiency ($\eta_{Tm–Yb}$) of the

$Tm^{3+} \rightarrow Yb^{3+}$ energy transfer can be calculated by using the following equation:[40]

$$\eta_{Tm-Yb} = 1 - \frac{\tau_{SA}}{\tau_S} \qquad (3)$$

where τ_{SA} (480 μs for LuGG1Tm1Yb; 310 μs for LuGG1Tm10Yb) is the lifetime of a sensitizer (S, Tm^{3+}) in the presence of an activator (A, Yb^{3+}) and τ_S (520 μs) is the lifetime of the sensitizer in the absence of the activator. The η_{Tm-Yb} is found to be 8% and 40% in LuGG1Tm1Yb and LuGG1Tm10Yb nano-garnets, respectively.

According to Dexter and Schulman theories on the energy transfer phenomenon in Ln^{3+} doped materials, quenching of luminescence is due to the energy transfer between two activators up to the energy sink in the lattice.[41] By considering the energy transfer between like centers, the average distance (R) between Tm^{3+}/Yb^{3+} ions can be expressed as:[42]

$$R = 2\left(\frac{3V}{4\pi C_{x+y}N}\right) \qquad (4)$$

where N is the number of sites that Ln^{3+} ions can occupy per unit cell (for garnets $N = 24$),[4] V is the volume of the unit cell, and C_{x+y} is the total doping concentration of x (Tm^{3+}) and y (Yb^{3+}) ions. It is found that in Tm^{3+} doped LuGG nano-garnets, 'R' is decreasing from 24.52 to 14.35 Å as C_x (Tm^{3+}) increases from 0.01 to 0.05, respectively (see Table 3). As shown in the inset of Fig. 5, the critical concentration of Tm^{3+} ions is 0.02 as the intensity is decreased beyond this concentration and the corresponding critical distance (R_0) is 19.47 Å. In the case of Tm^{3+}–Yb^{3+} co-doped nano-garnets, R is found to be around 19.4 and 10.96 Å for LuGG1Tm1Yb and LuGG1Tm10Yb nano-garnets, respectively.

The energy transfer from a sensitizer to an activator may take place *via* either exchange interaction or multipolar interaction.[7] The mechanism of exchange interaction plays no role in energy transfer between dopants since the exchange interaction is dominant only for short distances (typically <6 Å). In our case, the average distance between dopants is estimated to be 17.31 Å, which is higher compared to Ln^{3+} doped YAG single crystals (15.4 Å) and $Lu_3Al_5O_{12}$ garnets (16 Å), suggesting that the energy transfer through exchange interaction can be excluded.[43,44] Thus, the energy transfer in the present case will occur by electric multipolar interaction only.[7]

The presence of multipolar interactions leads to non-exponential decay. These interactions can be characterized by fitting the non-exponential decay curves to the Inokuti–Hirayama (IH) model.[45] Accordingly, the fluorescence decay intensity (I) is given by,

$$I(t) = I_0 \exp\left[-\left(\frac{t}{t_0}\right) - Q\left(\frac{t}{t_0}\right)^{\frac{3}{S}}\right] \qquad (5)$$

The intrinsic decay time of 1.0 mol% Tm^{3+} ions in LuGG nano-garnets is used as $\tau_0 = 590$ μs (is obtained by varying τ_0 and Q in fitting process) for which the energy transfer is negligible and the energy transfer parameter (Q) is defined as

$$Q = \frac{4\pi}{3}\Gamma\left(1 - \frac{3}{S}\right)N_0R_0^3 \qquad (6)$$

where $S = 6$, 8 or 10 for dipole–dipole, dipole–quadrupole or quadrupole–quadrupole interactions, respectively; N_0 is the concentration of activators; and R_0 is the critical transfer distance.

For LuGG1Tm, the decay curves of the $^3H_4$ level are well fitted to the IH model for $S = 6$, but the decay curves of other four singly Tm^{3+} doped LuGG nanogarnets are not well fitted to any value of S (6 or 8 or 10). For co-doped nano-garnets, the decay curves are well fitted to $S = 6$ indicating that there is a dipole–dipole interaction between Tm^{3+} and Yb^{3+} ions in the LuGG1Tm1Yb and LuGG1Tm10Yb nanogarnets with a Q value of 0.62 and 1.3, respectively. In the case of higher concentrations (>1.0 mol%) of Tm^{3+}-singly doped LuGG nano-garnets, the decay curves are not well-fitted to the IH model, which indicates that there could be some other energy transfer processes involved in the quenching of luminescence. In this regard diffusion limited energy transfer processes may also come into picture which causes a decrease in emission intensity and the corresponding lifetime of a particular emitting level.

In order to know the diffusion among active ions, the decay curves are fitted to the Martin model given by:[46]

$$I(t) = I(0) \exp\left[-\frac{t}{\tau_0} - Q\left(\frac{t}{\tau_0}\right)^{3/S}\left(\frac{1 + a_1X + a_2X^2}{1 + b_1X}\right)^{\frac{S-3}{S-2}}\right] \qquad (7)$$

where

$$Q = \frac{4\pi}{3}C_A\Gamma\left(1 - \frac{3}{S}\right)(C_{SA}\tau_0)^{3/S} \qquad (8)$$

$$X = BC_{SA}^{-2/S}t^{1-2/S} \qquad (9)$$

and τ_0 is the intrinsic lifetime, C_A is the activator concentration, Γ is the Euler function, C_{SA} and 'B' are the sensitizer–activator energy transfer and diffusion parameters, respectively. a_i and b_i are the Pade' approximate coefficients which are presented in Table 4.

Table 3 Dopant concentration (C), volume (V) and average distance (R) between dopants in Tm^{3+}/Yb^{3+}:LuGG nano-garnets

System	(C_{Tm+Yb})	V (Å³)	R (Å)
LuGG1Tm	0.01	1851.80	24.52
LuGG2Tm	0.02	1853.61	19.47
LuGG3Tm	0.03	1857.24	17.02
LuGG4Tm	0.04	1858.14	15.46
LuGG5Tm	0.05	1857.69	14.35
LuGG1Tm1Yb	0.02	1834.22	19.4
LuGG1Tm10Yb	0.11	1816.74	10.96

Table 4 Calculated values of Padé approximant coefficients in eqn (7) for different interactions

S	a_1	a_2	b_1
6	10.866	15.500	8.743
8	17.072	35.860	13.882
10	24.524	67.909	20.290

Table 5 The energy transfer parameter (Q) and diffusion parameter (B) obtained using the Martin model for the $^3H_4 \rightarrow {}^3H_6$ and $^1G_4 \rightarrow {}^3F_4$ transitions in Tm^{3+}/Yb^{3+}:$Lu_3Ga_5O_{12}$ nano-garnets

Label	$^3H_4 \rightarrow {}^3H_6$		$^1G_4 \rightarrow {}^3F_4$	
	Q	B	Q	B
LuGG1Tm	0.4	0	0.8	0
LuGG2Tm	1.27	0.0036	1.75	0.0035
LuGG3Tm	2.03	0.01	3.07	0.0099
LuGG4Tm	4.42	0.016	4.97	0.0137
LuGG5Tm	7.81	0.0189	7.18	0.008
LuGG1Tm1Yb	0.62	0	0.82	0
LuGG1Tm10Yb	1.3	0	1.14	0

The Martin model is well fitted to $S = 6$ for the decay curves of all the concentrations of Tm^{3+}-singly doped nano-garnets. The parameter Q is found to increase from 0.4 to 7.81 as Tm^{3+} concentration increases from 1.0 to 5.0 mol% (see Table 5 and Fig. 9(a)). As shown in the inset of Fig. 9(a), the diffusion parameter (B) increases from 0 to 0.0189 with increase in Tm^{3+} concentration from 1.0 to 5.0 mol%, and the values are shown in Table 5. In the case of Tm^{3+}/Yb^{3+} co-doped nano-garnets, it is observed that there is no diffusion between dopants ($B = 0$) and the same value for Q as in the IH model fitting is obtained. Hence, it can be concluded that the decrease in the emission intensity and effective lifetime of the $^3H_4$ level in the singly doped nano-garnets is due to the presence of CR energy transfer and diffusion processes, whereas in co-doped nano-garnets only CR energy transfer is the prime process quenching the emission and lifetime of the $^3H_4$ level.

**(ii) $^1G_4$ (Tm^{3+}) level.** The luminescence decay curves of the $^1G_4$ (Tm^{3+}) level for concentration dependent Tm^{3+}-singly doped LuGG (see Fig. 8) and Tm^{3+}–Yb^{3+} co-doped LuGG nano-garnets (not shown in figure) have been measured under laser excitation of the $^3H_6 \rightarrow {}^1G_4$ transition at 463 nm and

monitoring the emission at 650 nm corresponds to the $^1G_4 \rightarrow {}^3F_4$ transition. All the decay curves are found to be non-exponential in nature. The τ_{eff} of $^1G_4$ level has been calculated using eqn (2) and is found to decrease from 320 to 22 µs as Tm^{3+} concentration increases from 1.0 to 5.0 mol%, the values are shown in Table 2. The drastic decrease in the τ_{eff} of the $^1G_4$ level may be due to CR energy transfer and diffusion processes between Tm^{3+} ions. In co-doped nano-garnets, τ_{eff} is found to be around 290 and 270 µs in LuGG1Tm1Yb and LuGG1Tm10Yb nano-garnets, respectively. The τ_{eff} of the $^1G_4$ level is found to decrease with the addition of the Yb^{3+} ions into LuGG1Tm nano-garnets which could be due to energy transfer from Tm^{3+} to Yb^{3+}:$[^1G_4$ (Tm^{3+}), $^2F_{7/2}$ (Yb^{3+})] $\rightarrow$ $[^3H_5$ (Tm^{3+}), $^2F_{5/2}$ (Yb^{3+})]. It is also found that τ_{eff} of the $^1G_4$ level in LuGG nano-garnets is higher than those of Tm^{3+} doped $YAlO_3$, Y_2O_3, YPO_4, and $GdAl(BO_3)_4$ crystals and Tm^{3+}–Yb^{3+} co-doped Y_2BaZnO_5,YPO_4, and $GdAl(BO_3)_4$ crystals (see Table 2).[19,24–27,47] But they are lower than those of Tm^{3+} singly doped or Tm^{3+}–Yb^{3+} co-doped GGG nano-garnets which could be due to the competition between higher spontaneous emission and multiphonon relaxation rates ($1/\tau_0 = A + W_{MP}$) and the energy transfer probabilities when chemical pressure increases/decreases.[23]

The decay curves are fitted to the IH model and Martin model using eqn (5) and (7), respectively. Decay curves of the $^1G_4$ level of Tm^{3+} (>1.0 mol%) singly doped LuGG nano-garnets are not well fitted to the IH model for any value of S ($=6$ or 8 or 10), but in co-doped ones they are well fitted to $S = 6$ confirming dipole–dipole interaction between Tm^{3+} and/or Yb^{3+} ions. The Q values obtained from IH fitting are found to be 0.82 and 1.14 for LuGG1Tm1Yb and LuGG1Tm10Yb nano-garnets, respectively, which indicates the existence of energy transfer between Tm^{3+} and Yb^{3+} ions and the absence of
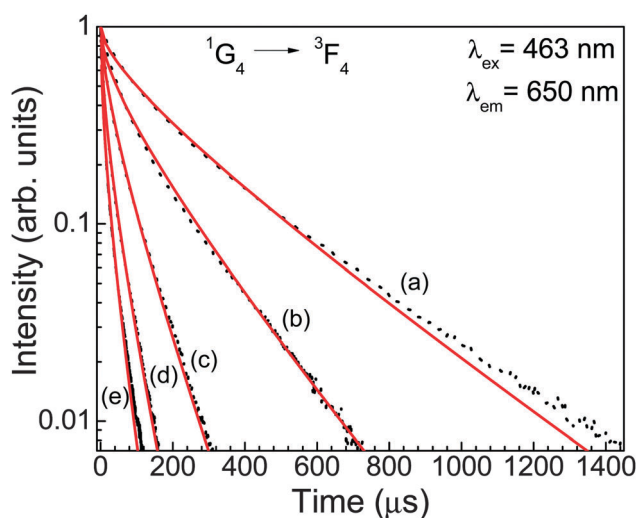
Fig. 8 Decay curves of the $^1G_4$ level of Tm^{3+} ions in (a) LuGG1Tm (b) LuGG2Tm, (c) LuGG3Tm, (d) LuGG4Tm and (e) LuGG5Tm nano-garnets under resonant excitation. The Martin model fitting (solid line) for $S = 6$ is shown for all nano-garnets.
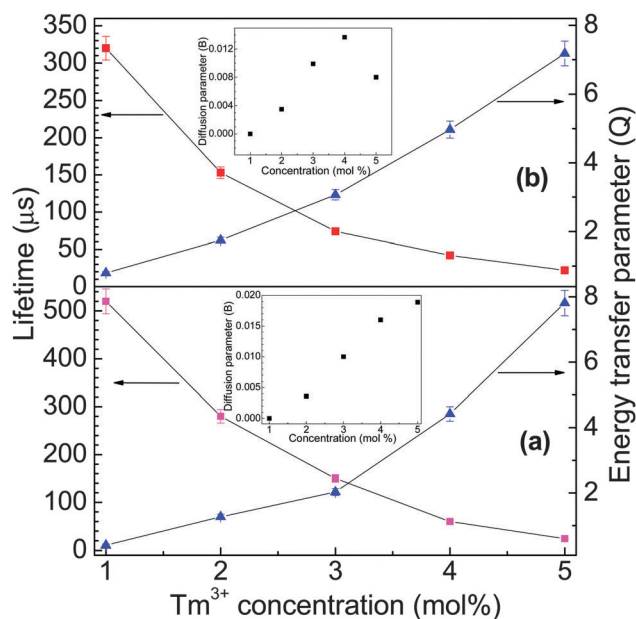
Fig. 9 Variation of the lifetime (■) and energy transfer parameter (▲) for (a) $^3H_4 \rightarrow {}^3H_6$ and (b) $^1G_4 \rightarrow {}^3F_4$ decay curves in LuGG nanogarnets, as a function of Tm^{3+} ion concentration. The inset shows the variation of the diffusion parameter with Tm^{3+} ion concentration.

14726 | *Phys. Chem. Chem. Phys.*, 2016, **18**, 14720–14729

This journal is © the Owner Societies 2016

diffusion between the dopants. The dipole–dipole interaction among Ln^{3+} ions increases with the chemical pressure since the Ln–Ln distances are reduced (Lu–Lu = 3.732 Å).[13] In order to know the diffusion process among active ions, the decay curves of Tm^{3+} singly-doped LuGG nano-garnets are fitted to the Martin model (well fitted to $S = 6$) and the Q value is found to increase from 0.8 to 7.18 as Tm^{3+} ion concentration increases from 1.0 to 5.0 mol%, respectively. As shown in the inset of Fig. 9(b), 'B' increases from 0 to 0.0137 as Tm^{3+} concentration increases from 1.0 to 4.0 mol% and then decreases to 0.008 for 5.0 mol%, and the values are tabulated (Table 5). It was reported that the energy transfer coefficients depend on sensitizer concentration and host material. Accordingly, at lower active-ion concentration, the energy transfer coefficients increase with concentration and then approach saturation at higher concentration of active-ions.[21] In the present work also, the saturation of energy transfer is found for higher Tm^{3+} concentrations (>4.0 mol%).

(iii) $^2F_{5/2}$ (Yb^{3+}) level. In both co-doped nano-garnets, decay curves of the $^2F_{5/2}$ (Yb^{3+}) level were measured with 930 nm laser excitation and are shown in Fig. 10. The decay curve of the $^2F_{5/2}$ level in LuGG1Tm1Yb nano-garnets exhibits a slight non-exponential nature with a lifetime of 390 μs. Upon doping 10 mol% of Yb^{3+} ions into the LuGG1Tm nano-garnets, the decay curve of the $^2F_{5/2}$ level exhibits non-exponential nature with a lifetime of 60 μs. The $^2F_{5/2}$ level decay curves of LuGG1Tm1Yb and LuGG1Tm10Yb nano-garnets are well fitted to the IH model and the Martin model, respectively; with 425 μs as the intrinsic lifetime (this value is obtained by varying τ_0 and Q in IH fitting for LuGG1Tm1Yb nano-garnets). The energy transfer parameter Q is found to be 0.17 and 0.13 and the diffusion parameter B is found to be 0 and 1.867 for LuGG1Tm1Yb and LuGG1Tm10Yb, respectively. This indicates that $Yb^{3+} \rightarrow Tm^{3+}$ energy transfer is dominant at lower concentration whereas at a higher concentration of Yb^{3+} ions, the diffusion process is predominant in shortening the lifetime of

the $^2F_{5/2}$ level. In the absence of energy transfer (no Tm^{3+} co-doping), the lifetime (λ_{exc} = 930 nm) of the $^2F_{5/2}$ level in LuGG:Yb^{3+} was found to be 1040 μs.[17] By using eqn (3), the efficiency of the $Yb^{3+} \rightarrow Tm^{3+}$ energy transfer (η_{Yb-Tm}) can be calculated, where τ_{DA} (390 μs) is the lifetime of the sensitizer (S, Yb^{3+}) in the presence of the activator (A, Tm^{3+}) and τ_D (1040 μs) is the lifetime of the sensitizer in the absence of the activator. The η_{Yb-Tm} is found to be 62% and 94% for LuGG1Tm1Yb and LuGG1Tm10Yb nano-garnets, respectively.

3.5. Upconversion

Upconversion (UC) is a kind of anti-Stokes emission that converts two or more low energy photons into a high energy photon and this can be obtained by either excited state absorption (ESA) and/or energy transfer upconversion (ETU). The UC by sensitized ETU is the most efficient mechanism for Tm^{3+}–Yb^{3+} co-doped samples, since there is no absorption band at 970 nm for Tm^{3+} ions (see Fig. 3). Fig. 11 shows the blue upconverted emission in the 440–530 nm region, and red upconverted emission is in the region of 620–700 nm, assigned to the $^1G_4 \rightarrow {}^3H_6$ and $^1G_4 \rightarrow {}^3F_4$ transitions, respectively, which were obtained under 970 nm laser excitation. To analyze the UC processes, the upconverted emission intensities were recorded as a function of pump power. As a result, the upconverted emission intensity (I_{UP}) follows the relation: $I_{UP} \propto (I_{IR})^n$, where '$I_{IR}$' is the IR excitation intensity, 'n' is the number of IR photons absorbed per emitted photon.[4] The slope values for blue and red emissions are found to be 2.34 and 2.22, respectively, in LuGG1Tm1Yb nano-garnets (see inset of Fig. 11). In LuGG1Tm10Yb nano-garnets, the slopes are found to be 1.66 and 1.64 for blue and red emissions, respectively. Except the slope for red emission in LuGG1Tm1Yb nano-garnets,
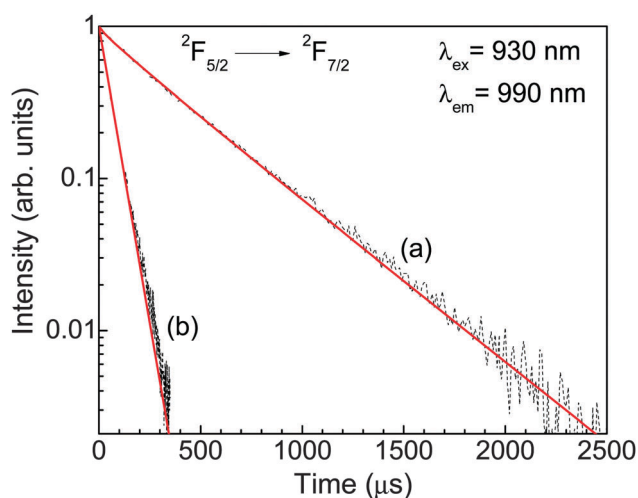

Fig. 10 Decay curves of the $^2F_{5/2}$ level of Yb^{3+} ions in (a) LuGG1Tm1Yb and (b) LuGG1Tm10Yb nano-garnets under resonant excitation. The solid line is the IH fitting (a) and Martin fitting (b) for $S = 6$.
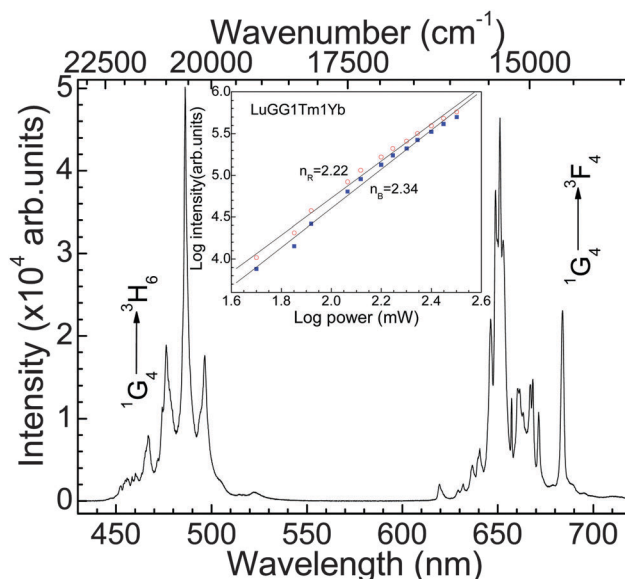

Fig. 11 Upconversion spectra of LuGG1Tm1Yb nano-garnets at λ_{exc} = 970 nm and laser power = 317 mW. The inset shows the log–log plot of blue [■] and red [○] UC emission as a function of pumping power. (n_R = slope for red emission, n_B = slope for blue emission).

This journal is © the Owner Societies 2016

Phys. Chem. Chem. Phys., 2016, **18**, 14720–14729 | **14727**

other slope values in both the nano-garnets are deviated from the expected values (blue = 3) due to infinitely large UC rates.[48]

The upconverted emission from Tm^{3+} ions and a simple schematic representation of Yb^{3+} to Tm^{3+} energy transfer processes are depicted in the right side of Fig. 4. Following the absorption of the 970 nm pump photon, the Yb^{3+} ions are excited from the $^2F_{7/2}$ to the $^2F_{5/2}$ level, which then non-resonantly transfers its energy (ET1) to the ground state Tm^{3+} ions and excite them from the $^3H_6$ ground state to the $^3H_5$ excited state where the excess energy (~ 1600 cm^{-1}) can be dissipated to the LuGG lattice in the form of phonons. Multi-phonon relaxation in turn populates the $^3F_4$ state. The Tm^{3+} ions are then resonantly excited to the $^3F_2$ state *via* ET2, and then they decay non-radiatively to the $^3H_4$ level *via* the $^3F_3$ level. Simultaneously, another excited Yb^{3+} ion in close proximity can also transfer its energy non-resonantly to the Tm^{3+} ion which is in the $^3H_4$ level and excites to the $^1G_4$ level (ET3). The excess energy (~ 1800 cm^{-1}) can be dissipated to the LuGG lattice. This in turn leads to the intense blue ($^1G_4 \rightarrow {}^3H_6$) and red ($^1G_4 \rightarrow {}^3F_4$) emissions. The considerable blue and weak red upconverted emissions were reported in Tm^{3+}–Yb^{3+} co-doped $Lu_5O_4F_7$, LuF_3, YAG, GGG, Lu_2O_3 nanocrystals and $La_2(MoO_4)_3$ micro-architectures under ~ 980 nm laser excitation.[11,12,22,23,26,49] In the as-synthesized LuGG1Tm1Yb nano-garnets, we observed more intense and wider range upconverted blue and red emissions.

4. Conclusions

Tm^{3+} doped and Tm^{3+}–Yb^{3+} co-doped $Lu_3Ga_5O_{12}$ nano-garnets were synthesized in the single phase of cubic structure with an average crystallite size of about 30 nm. The dynamic light scattering technique confirms that the particle size distribution of the nano-garnets is in the 15–90 nm range. Under 473 nm laser excitation, weak red and intense near infrared Stokes emissions are observed in Tm^{3+}-doped and Tm^{3+}–Yb^{3+} co-doped $Lu_3Ga_5O_{12}$ nano-garnets. Decay curves of the $^3H_4$ and $^1G_4$ (Tm^{3+}) levels exhibit non-exponential nature and their effective lifetimes are found to decrease with increase in Tm^{3+} ion concentration as well as upon co-doping with Yb^{3+} ions. Analysis of non-exponential decay curves using the generalized Yokota–Tanimoto model confirms dipole–dipole interaction among optically active ions. The $Yb^{3+} \rightarrow Tm^{3+}$ energy transfer is dominant at low Yb^{3+} concentration, whereas at higher Yb^{3+} concentration, energy diffusion is predominant in shortening the lifetime of the $^2F_{5/2}$ level. The intense blue anti-Stokes luminescence has been observed in Tm^{3+}–Yb^{3+} co-doped $Lu_3Ga_5O_{12}$ nano-garnets due to the energy transfer upconversion mechanism. The results emphasise that the nano-garnets are more desirable candidates for photonic device applications.

Acknowledgements

References

1 F. Wang and X. Liu, in *Rare-Earth Doped Upconversion Nanophosphors*, ed. D. L. Andrews, G. D. Scholes and G. P. Wiederrecht, Compreh. Nanosci. and Tech., 2011, vol. 1, p. 607.

2 S. F. León-Luis, V. Monteseguro, U. R. Rodríguez-Mendoza, M. Rathaiah, V. Venkatramu, A. D. Lozano-Gorrín, R. Valiente, A. Muñoz and V. Lavín, *RSC Adv.*, 2014, **4**, 57691.

3 V. Venkatramu, M. Giarola, G. Mariotto, S. Enzo, S. Polizzi, C. K. Jayasankar, F. Piccinelli, M. Bettinelli and A. Speghini, *Nanotech.*, 2010, **21**, 175703.

4 V. Venkatramu, S. F. León-Luis, U. R. Rodríguez-Mendoza, V. Monteseguro, F. J. Manjón, A. D. Lozano-Gorrín, R. Valiente, D. Navarro-Urríos, C. K. Jayasankar, A. Muñoz and V. Lavin, *J. Mater. Chem.*, 2012, **22**, 13788.

5 X. Huang, S. Han, W. Huang and X. Liu, *Chem. Soc. Rev.*, 2013, **42**, 173.

6 S. Ganguli, C. Hazra, M. Chatti, T. Samanta and V. Mahalingam, *Langmuir*, 2016, **32**, 247.

7 G. K. Liu and B. Jacquier, *Spectroscopic Properties of Rare Earths in Optical Materials*, Tsinghua University Press, Springer, Berlin, 2005.

8 R. N. Bhargava, D. Gallagher, X. Hong and A. Nurmikko, *Phys. Rev. Lett.*, 1994, **72**, 416.

9 Y. Song, H. You, Y. Huang, M. Yang, Y. Zheng, L. Zhang and N. Guo, *Inorg. Chem.*, 2010, **49**, 11499.

10 F. T. Rabouw, S. A. den Hartog, T. Senden and A. Meijerink, *Nat. Commun.*, 2014, **5**, 3610.

11 W. Luo, Y. Wang, Y. Chen, T. Wen, M. Liu, Y. Wang, F. Liao and J. Lin, *J. Mater. Chem. C*, 2013, **1**, 5711.

12 S. Xiao, X. Yang, J. W. Ding and X. H. Yan, *J. Phys. Chem. C*, 2007, **111**, 8161.

13 V. Monteseguro, M. Rathaiah, K. Linganna, A. D. Lozano-Gorrín, M. A. Hernández-Rodríguez, I. R. Martín, P. Babu, U. R. Rodríguez-Mendoza, F. J. Manjón, A. Muñoz, C. K. Jayasankar, V. Venkatramu and V. Lavín, *Opt. Mater. Express*, 2015, **5**, 1661.

14 M. Rathaiah, P. Haritha, K. Linganna, V. Monteseguro, I. R. Martín, A. D. Lozano-Gorrín, P. Babu, C. K. Jayasankar, V. Lavín and V. Venkatramu, *ChemPhysChem*, 2015, **16**, 3928.

15 C. Maunier, J. L. Doualan, R. Moncorge, A. Speghini, M. Bettinelli and E. J. Cavalli, *J. Opt. Soc. Am. B*, 2002, **19**, 1794.

16 O. Guillot-Noel, B. Bellamy, B. Viana and D. Gourier, *Phys. Rev. B: Condens. Matter Mater. Phys.*, 1999, **66**, 1668.

17 W. Han, K. Wu, X. Tian, L. Xia, H. Zhang and J. Liu, *Opt. Mater. Express*, 2013, **3**, 920.

18 B. Bitnar, *Semicond. Sci. Technol.*, 2003, **18**, S221.

19 W. Zheng, H. Zhu, R. Li, D. Tu, Y. Liu, W. Luo and X. Chen, *Phys. Chem. Chem. Phys.*, 2012, **14**, 6974.

20 J. Ganem, J. Crawford, P. Schmidt, N. W. Jenkins and S. R. Bowman, *Phys. Rev. B: Condens. Matter Mater. Phys.*, 2002, **66**, 245101.

21 Y. Mita, T. Ide, M. Togashi and H. Yamamoto, *J. Appl. Phys.*, 1999, **85**, 4160.

22 M. Liu, S. W. Wang, J. Zhang, L. Q. An and L. D. Chen, *Opt. Mater.*, 2007, **30**, 370.

23 F. Pandozzi, F. Vetrone, J. C. Boyer, R. Naccache, J. A. Capobianco, A. Speghini and M. Bettinelli, *J. Phys. Chem. B*, 2005, **109**, 17400.

24 H. Manaa, V. Wiedeman, R. Moncorgé, M. Koselja and J. C. Souriau, *J. Phys. IV*, 1994, **4**, C4-525.

25 F. Vetrone, J. C. Boyer, J. A Capobianco, A. Speghini and M. Bettinelli, *Nanotech.*, 2004, **15**, 75.

26 L. An, J. Zhang, M. Liu and S. Wang, *J. Alloys Compd.*, 2008, **451**, 538.

27 I. Etchart, I. Hernandez, A. Huignard, M. Berard, M. Laroche, W. P. Gillin, R. J. Curry and A. K. Cheetham, *J. Appl. Phys.*, 2011, **109**, 063104.

28 H. M. Rietveld, *J. Appl. Crystallogr.*, 1969, **2**, 65.

29 J. Rodríguez-Carvajal, *Physica B*, 1993, **192**, 55.

30 D. Li, Y. Wang, X. Zhang, H. Dong, L. Liu, G. Shi and Y. Song, *J. Appl. Phys.*, 2012, **112**, 094701.

31 Ł. Dobrzycki, E. Bulska, D. A. Pawlak, Z. Frukacz and K. Woźniak, *Inorg. Chem.*, 2004, **43**, 7656.

32 R. Pecora, *Dynamic light scattering: Applications of photon correlation spectroscopy*, Plenum press, New York, 1985.

33 G. H. Deike, *Spectra and Energy levels of Rare earth ions in crystals*, Inter Science Publishers, New York, 1968.

34 J. Li, J. Zhang, Z. Hao, X. Zhang, J. Zhao and Y. Luo, *J. Appl. Phys.*, 2013, **113**, 223507.

35 G. Boulon, L. Laversenne, C. Goutaudier, Y. Guyot and M. T. Cohen-Adad, *J. Lumin.*, 2003, **102–103**, 417.

36 G. Armagan, A. M. Buoncristiani and B. Di Bartolo, *Opt. Mater.*, 1992, **1**, 11.

37 F. S. Ermeneux, C. Goutaudier, R. Moncorg, M. T. Cohen-Adad, M. Bettinelli and E. Cavalli, *Opt. Mater.*, 1997, **8**, 83.

38 H. Lin, S. Zhou, X. Hou, W. Li, Y. Li, H. Teng and T. Jia, *IEEE Photonics Technol. Lett.*, 2010, **22**, 866.

39 G. Dominiak-Dzik, W. Ryba-Romanowski, R. Lisiecki, I. Foldvári and E. Beregi, *Opt. Mater.*, 2009, **31**, 989.

40 D. F. de Sousa, F. Batalioto, M. J. V. Bell, S. L. Oliveira and L. A. O. Nunes, *J. Appl. Phys.*, 2001, **90**, 3308.

41 D. L. Dexter and J. H. Schulman, *J. Chem. Phys.*, 1954, **22**, 1063.

42 G. Blasse, *Philips Res. Rep.*, 1969, **24**, 131.

43 J. Shmulovich, G. W. Berkstresser and D. Brasen, *J. Chem. Phys.*, 1985, **82**, 3078.

44 A. A. Setlur, J. J. Shiang and C. J. Vess, *J. Phys. Chem. C*, 2011, **115**, 3475.

45 M. Inokuti and F. Hirayama, *J. Chem. Phys.*, 1965, **43**, 1978.

46 I. R. Martín, V. D. Rodríguez, U. R. Rodríguez-Mendoza, V. Lavín, E. Montoya and D. Jaque, *J. Chem. Phys.*, 1999, **111**, 1191.

47 Q. Y. Zhang, G. F. Yang and Z. H. Jiang, *Appl. Phys. Lett.*, 2007, **91**, 051903.

48 M. Pollnau, D. R. Gamelin, S. R. Luthi, H. U. Gudel and M. P. Hehlen, *Phys. Rev. B: Condens. Matter Mater. Phys.*, 2000, **61**, 3337.

49 Z. Chen, W. Bu, N. Zhang and J. Shi, *J. Phys. Chem. C*, 2008, **112**, 4378.

This journal is © the Owner Societies 2016

Phys. Chem. Chem. Phys., 2016, **18**, 14720–14729 | **14729**